Int. J. Electrochem. Sci., 13 **(2018)** 6112 – 6125, doi: 10.20964/2018.06.38

International Journal of ELECTROCHEMICAL SCIENCE
www.electrochemsci.org

Proton Ion Conducting Solid Polymer Electrolytes Based on Chitosan Incorporated with Various Amounts of Barium Titanate ($BaTiO_3$)

Shujahadeen B. Aziz[1,2,*], *Wrya O. Karim*[3], *Karwan W. Qadir*[4,5], *Qayyum Zafar* [6]

[1] Advanced Polymeric Materials Research Lab., Department of Physics, College of Science, University of Sulaimani, Qlyasan Street, Sulaimani, Kurdistan Regional Government-Iraq
[2] Komar Research Center (KRC), Komar University of Science and Technology, Sulaimani, 46001, Kurdistan Regional Government, Iraq
[3] Department of Chemistry, College of Science, University of Sulaimani, Qlyasan Street, Sulaimani, Kurdistan Regional Government-Iraq
[4] Department of Physics, College of Education, Salahaddin University-Hawler, 44001 Erbil, Kurdistan Region, Iraq.
[5] Physics Education Department, Faculty of Education, Ishik University, 44001 Erbil, Iraq.
[6] Department of Physics, Government College University, Lahore 54000, Pakistan.

[*]E-mail: shujaadeen78@yahoo.com, shujahadeenaziz@gmail.com

Received: 15 February 2018 / *Accepted:* 10 April 2018 / *Published:* 10 May 2018

Here the impact of barium titanate ($BaTiO_3$) nano filler on both electrical and dielectric properties of proton conducting solid polymer electrolytes based on chitosan have been discussed using AC impedance spectroscopy. The impedance data reveals that up to 3 wt. % of $BaTiO_3$, the conductivity shows an increaseAt low frequency, the maximum values for both dielectric constant and dielectric loss have been observed. Further distinguishable peaks have been observed in the imaginary part of electric modulus while no such peaks were observed in dielectric loss spectra From the Argand plots, the relaxation processes was interpreted. At low temperature, the DC conductivity versus reciprocal of temperature obeys the Arrhenius equation and at the high temperature, the curvature was obtained as an evidence for ion transport process with the aid of polymer segmental motion. Grotthus mechanism was used to interpret the conductivity behaviors of the samples.

Keywords: Polymer Composite, barium titanate, Proton Ion Conductor, Relaxation process, Arhenius and VTF equations

1. INTRODUCTION

Ion conducting polymers obtained from the dissolved salts in functional polymers is becoming increasingly important; because of their application in solid-state polymer batteries and fuel cells [1]. In particular, extensive R&D efforts are being directed towards solid electrolytes for their use in batteries, owing to their high performance, durability, cost-effectiveness, portability, and mechanical flexibility [2]. At present ion conducting polymers exhibit low conductivity, thermal instability and mechanical weakness. The ubiquitous strategy to overcome these issues is the incorporation of nano-sized fillers to polymer electrolytes in an effort to decrease the concentration of crystalline phases without damaging the polymer flexibility and the mechanical stability over a wide temperature range [3, 4, 5]. The well reported achievement is that the synthesized polymer composite electrolytes must have both higher ionic conductivity and the desirable mechanical property [6]. Both the heterogeneous doping and percolation theories can guide researchers to enhance transport property. One of the attempts is the particle dispersion in polymer electrolytes by which the highly conductive interfaces could be produced in terms of the Lewis acid-base interactions between the surface states of fillers with both the polymer chains and ions. Once the percolation of these interfaces occurs, the transport properties will be significantly improved and the Lewis acid-base interactions may also hinder the crystallization of the polymer [4, 7, 8]. Among the various kinds of ion-conducting polymers, proton-conducting polymers have been extensively studied by virtue of their possible use in Proton Exchange Fuel Cells (PEFCs) which supply clean energy for automotives [9]. Interestingly the study of proton conduction in solids dates back to the fact that ice conducts electricity. Subsequently, the study of proton-conducting materials and the investigation of proton conductivity have been expanded to both proton-conducting polymer electrolytes for and proton-conducting oxides for applications below and above 100 ^{o}C [10]. In general, proton-conducting polymers are usually based on polymer electrolytes, comprising negatively charged groups attached to the polymer backbone. These polymer electrolytes tend to be rather rigid and of poor proton conductivity unless they are wetted [11]. Proton conducting polymer electrolytes containing different acids/salts and polymers have been reported by various authors [9, 11, 12]. Generally, ceramic fillers are classified into two types: active and passive. The active ceramic materials participate in the conduction process, for example, Li_2N and $LiAl_2O_3$, while the later ones have not been involved in the lithium transport process, such as Al_2O_3, SiO_2, $BaTiO_3$ and MgO. The size and features of the filler influence the electrochemical properties of the polymer electrolytes [13]. Among the inactive (i.e., non-ion conducting materials) inorganic fillers, aluminum oxide (Al_2O_3), silicon oxide (SiO_2), and titanium oxide (TiO_2) are the most commonly studied fillers [14]. The main objective of the present work is to investigate the electrical properties of the chitosan - $BaTiO_3$ nanocomposite. The present work explains the electrical properties of chitosan solid electrolyte as a function of varied $BaTiO_3$ contents in the composite film, using AC impedance spectroscopy. Based on the results of DC conductivity and dielectric constant the possible mechanism of ion conduction in these composite films is presented.

2. EXPERIMENTAL DETAILS

2.1 Sample Preparation and Electrical Characterizations

2.1.1 Chemicals

In our study, chitosan from crab shells (≥75% deacetylated, average molecular weight 1.1×10^5), 99% pure ammonium triflate ($NH_4CF_3SO_3$) and 99.9% pure barium titanate nanopowder ($BaTiO_3$, size < 50 nm) have been purchased commercially from Sigma-Aldrich. The solvent glacial acetic acid has also been obtained from Sigma Aldrich.

2.1.2 Sample preparations and Electrical Characterization technique

Acetic acid (1 %) was prepared by dilution of glacial acetic acid solution and was further used as the solvent to prepare the nano-composite solid polymer electrolytes. In general, the proton ion conducting films were prepared using single solvent by the solution cast technique. For this purpose, 1 gm of chitosan (CS) was primarily dissolved in 100 ml of 1% acetic acid solution. The mixture was stirred overnight at room temperature to ensure complete dissolution of chitosan powder in the acetic acid solution. Later, 30 wt. % $NH_4CF_3SO_3$ (NH_4Tf) was added to the CS solution and was subjected to continuous stirring until homogeneous chitosan:$NH_4CF_3SO_3$ (CS:NH_4Tf) solution was obtained. For the preparation of nano-composite polymer electrolytes, $BaTiO_3$ (BT) filler with varied concentrations (1, 3 and 5 wt. %) was dispersed in 20 ml acetic acid solution. The $BaTiO_3$ dispersions were later mixed with the CS:NH_4Tf solution followed by continuous stirring. The series of resulting solutions were designated as NPE1, NPE2, and NPE3 for CS:NH_4Tf solution incorporated with 1wt.%, 3 wt. % and 5wt. % of $BaTiO_3$ filler, respectively. Whereas, pure chitosan solution was designated as NPE0. The films were obtained by drying the NPE0, NPE1, NPE2, and NPE3 solutions in pre-cleaned Petri dishes under ambient conditions. To ensure complete drying, the films were peeled and placed in desiccator with blue silica gel desiccant. The facile procedure yielded free standing and mechanically stable films.

To study the ionic conductivity of the samples, films were mounted on the conductivity holder with blocking stainless steel disk electrodes (diameter = 2 cm). During the electrical characterization, the impedance data acquisition was performed by using computer interfaced HIOKI 3531 Z Hitester. The study was carried out in the operational frequency range of 50 Hz – 1 MHz, in the temperature range ~ 303 to 363 K.

3. RESULTS AND DISCUSSION

3.1 Impedance Study

Impedance spectroscopy is one of the powerful techniques used to study the ionic conductivity of polymeric materials [15]. Using this technique, the inter-particle interaction such as grain and grain boundary effects may be facilely determined with the aid of complex impedance formalism [16]. The

interpretation of data points from the impedance plots which almost forms a curvature can be attributed to grain boundaries as shown in *Fig. 1* [17, 18].

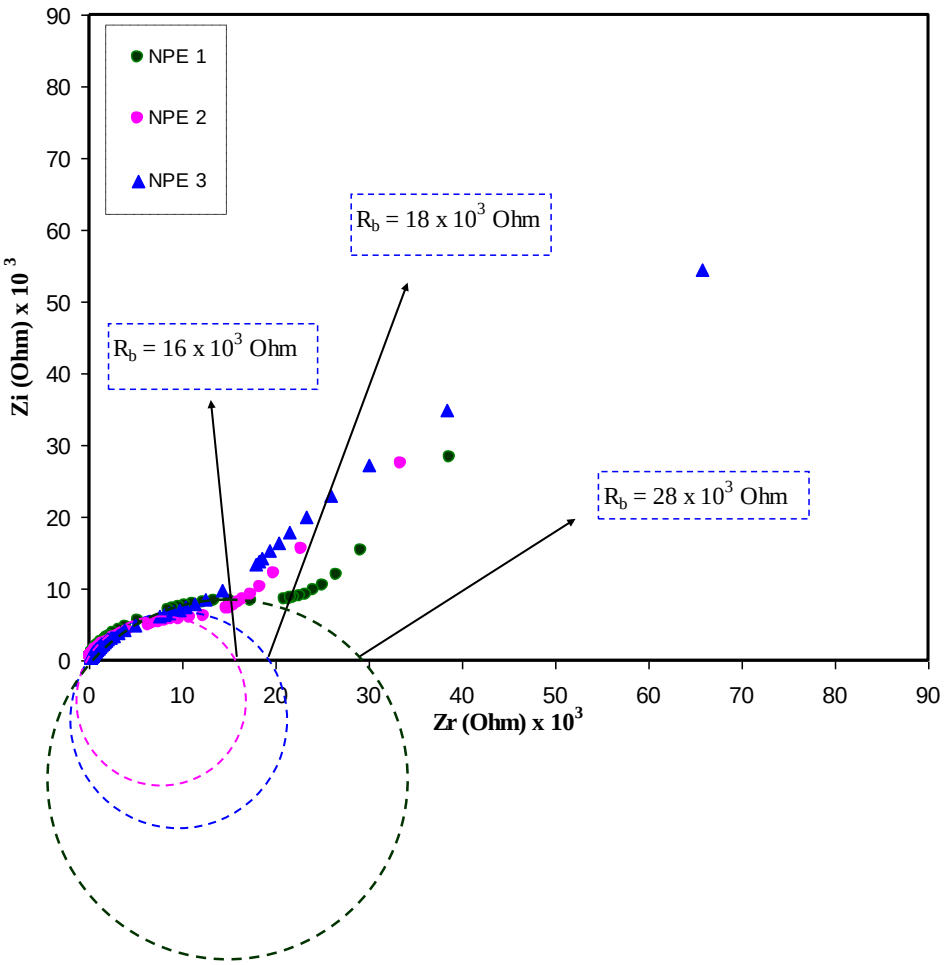

Figure 1. Impedance plots for all the composite solid films at room temperature.

An increase in filler content results in the agglomeration of the grains, causing some of the existing conducting pathways to be blocked, which ultimately results in decrease in conductivity [13]. In the present study, the centers of the semi-circles have been observed to be below the Z_r axis, suggesting that the relaxation of ions in the fabricated samples is non-Debye type [19]. The inset of the impedance plots also depicts the bulk resistance (R_b) of all the samples. It may be clearly observed from the inset of *Fig.1* that the NPE2 sample (with 3 wt. % $BaTiO_3$ incorporation) exhibits a minimum resistance of 16 kΩ. However, with 5 wt. % $BaTiO_3$ incorporation, the maximum resistance of the sample has been observed to increase to 28 kΩ.

3.2 Dielectric constant Study

Dielectric spectroscopy is a key tool for probing the dielectric properties of the medium as a function of frequency. The frequency spectrum of the complex susceptibility ($\varepsilon = \varepsilon' - i\varepsilon''$) provides

information about interaction of electric dipole with external field. The resulting data may also be used to estimate the ac conductivity of the material in a given frequency range. *Figure 2 and 3*; depict the dielectric constant and dielectric loss versus frequency for the fabricated samples at ambient temperature. In the present study, the dielectric constant has been extracted from the real (Z_r) and imaginary (Z_i) part of the complex impedance (Z*), using the following equations [20, 21]:

$$\varepsilon_r = \frac{Z_i}{\omega C_\circ (Z_r^{\,2} + Z_i^{\,2})} \qquad (1)$$

$$\varepsilon_i = \frac{Z_r}{\omega C_\circ (Z_r^{\,2} + Z_i^{\,2})} \qquad (2)$$

Where $C_o = \varepsilon_o A/t$ is the vacuum capacitance, ε_o=8.85×10^{-12} F/m is the permittivity of free space and $\omega = 2\pi f$ is the angular frequency and f is the applied field frequency. It may be observed from Fig. 2 and 3 that in low frequency region dispersion appears in both dielectric constant and loss spectra. From this region, the large value for both dielectric constant and dielectric loss has been obtained which may be ascribed to the space charge polarization near electrode-electrolyte interface [22]. Moreover, at low frequency region, the dipoles and charge carriers have sufficient time to orient in the direction of the applied electric field. Consequently, accumulation of charge carriers at the electrode/electrolyte interface results in the electrode polarization, which suppresses the high frequency dielectric properties (bulk property) [4, 21, 23]. It is clear that the dielectric loss value is larger than that of dielectric constant, relating to the contribution of carrier motion (DC conductivity) to the dielectric loss values [24, 25, 26].

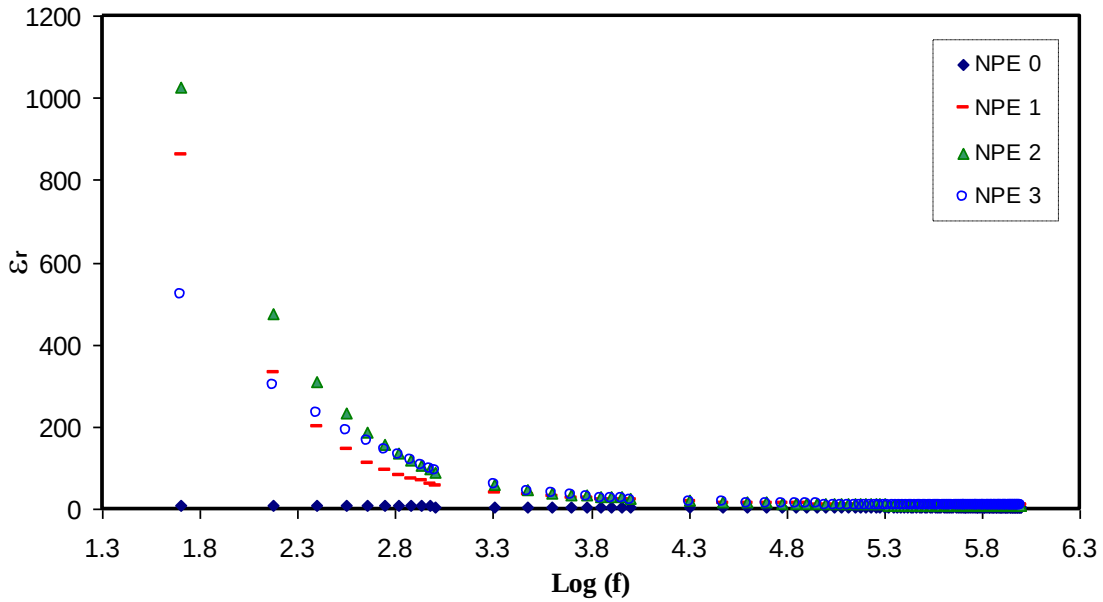

Figure 2. Dielectric constant versus logarithmic frequency for the fabricated samples at room temperature.

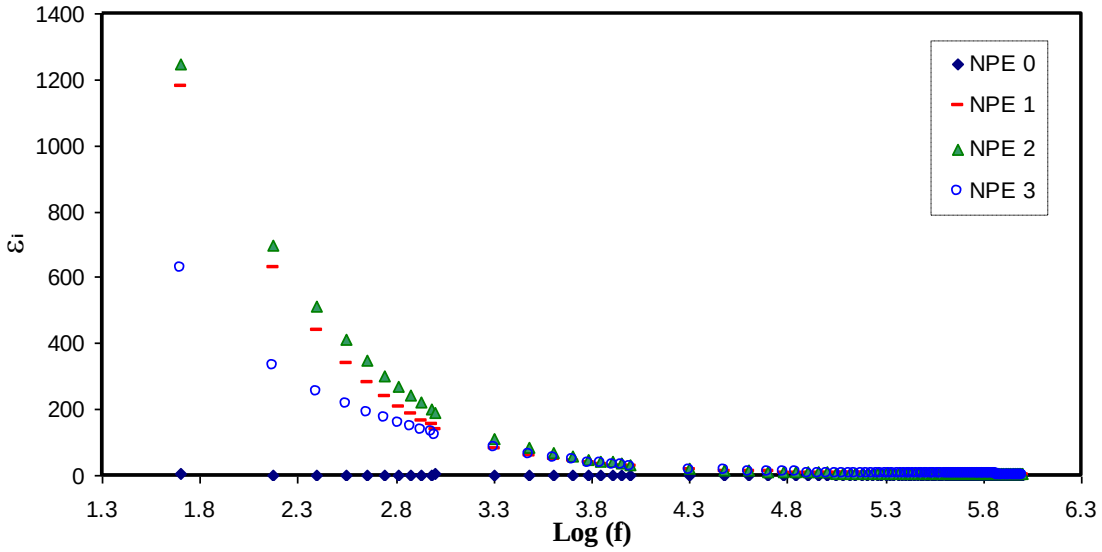

Figure 3. Dielectric losses versus logarithmic frequency for the fabricated samples at room temperature.

It may also be observed from Fig. 2 and 3 that the dielectric constant and loss factor decrease significantly with an increase in frequency. The high frequency region may be featured as a smooth plateau region (as depicted in Fig. 4) representing the bulk property of the fabricated samples [27]. Figure 5 plots the estimated dielectric constants of the composite films with various $BaTiO_3$ concentrations. It may be noticed that the dielectric constant increases with increasing $BaTiO_3$ concentration up to 3 wt. %, and subsequently decreases with further addition of the filler. The increase of dielectric constant with the addition of $BaTiO_3$ filler may be explained on the basis of space charge-model.

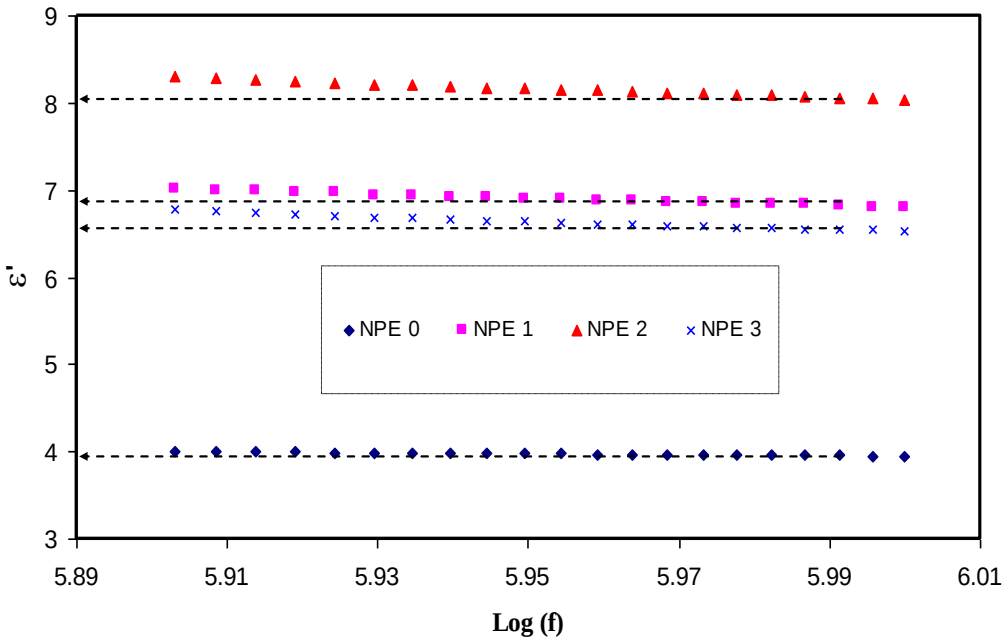

Figure 4. high frequency region of dielectric constant versus frequency for all the samples at ambient temperature.

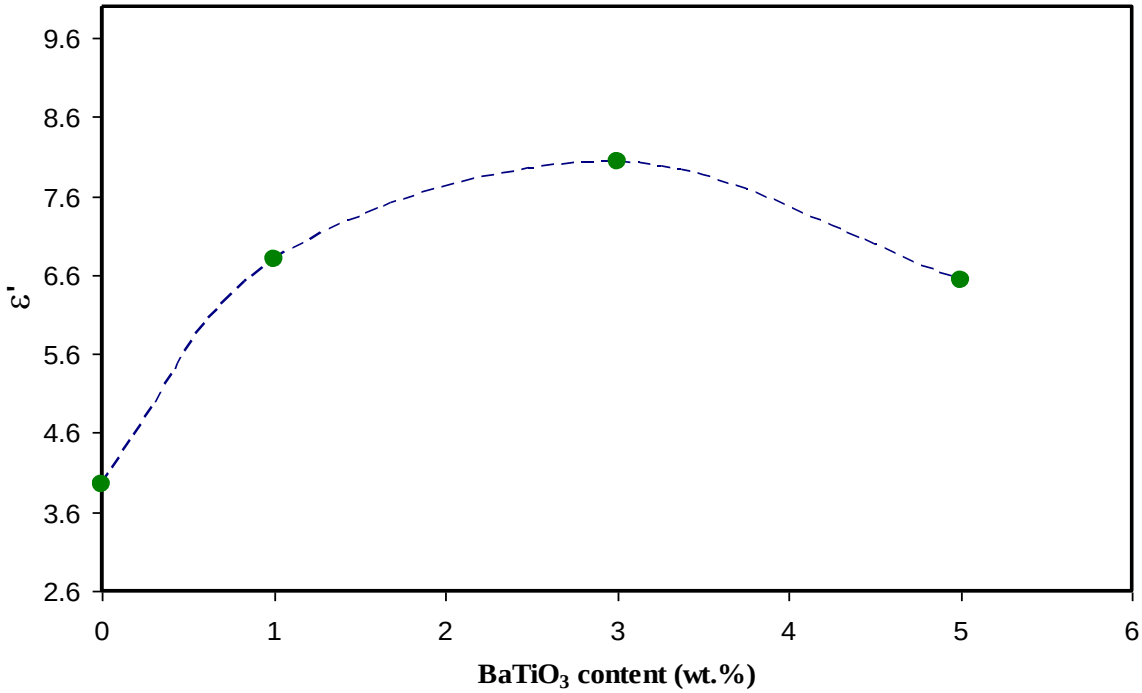

Figure 5. Dielectric constant versus $BaTiO_3$ filler concentration at room temperature.

According to this model, the high conducting interfacial layers on the surface of grains overlaps on each other which provides high conducting pathways for free ions and thus assist the ions transport [4, 5, 28, 29]. These highly conducting pathways are expected to increase with an increase in the concentration of $BaTiO_3$ filler. At still higher concentration though, the dielectric constant drops down due to the blocking effect which hinders the motion of ions, thereby leading to lower conductivity value [12, 29]. This observation may be related to the fact that the dispersion of 5 wt. % $BaTiO_3$ grains may cause the long polymer chains to be be immobilized leading to a decrease in dielectric constant and conductivity as well [5, 30].

3.3 Electric Modulus Study

The electrode polarization (EP), space charge injection phenomena and conduction effects obscure relaxation in dielectric permittivity presentation. Despite of the complexity of interpretation of these ambiguous phenomena, all these can be resolved in electric modulus formalism [29, 31]. The appropriate modulus that is useful in understanding bulk relaxation properties at low frequency region is the electric modulus. The real (Z_r) and imaginary (Z_i) parts of complex impedance (Z^*) may be used for the evaluation of real and imaginary parts of electric modulus, using the following equations [32]:

$$M_r = \omega C_o Z_i \quad (3)$$

$$M_i = \omega C_o Z_r \quad (4)$$

Fig. 6 reveals low and high values for M_r at low and high frequency regions, respectively for all the fabricated samples. From *Fig. 6*, it can be observed that the M_r value approaches to zero at low frequencies. This is due to the high value of capacitance associated with double layer charges build up between the sample and electrodes [33, 34]. It is noteworthy that in comparison to dielectric constant pattern, the M_r spectrum behaves in different manner. This is owing to the fact that the complex electric modules (M_r and M_i) are the reciprocal of complex dielectric constant.

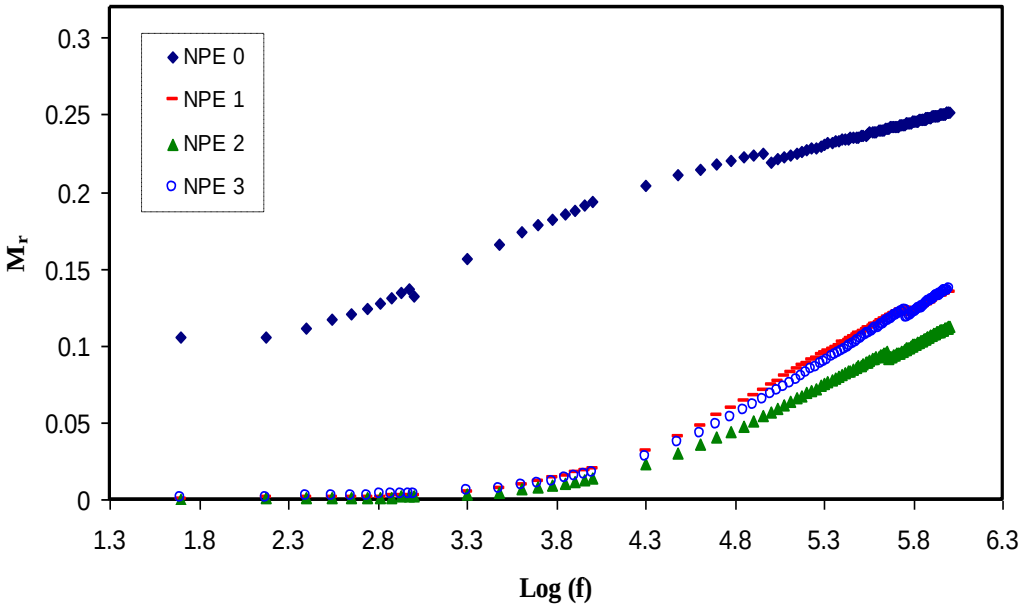

Figure 6. The real part of electric modules (M_r) as a function of frequency, for all the fabricated samples.

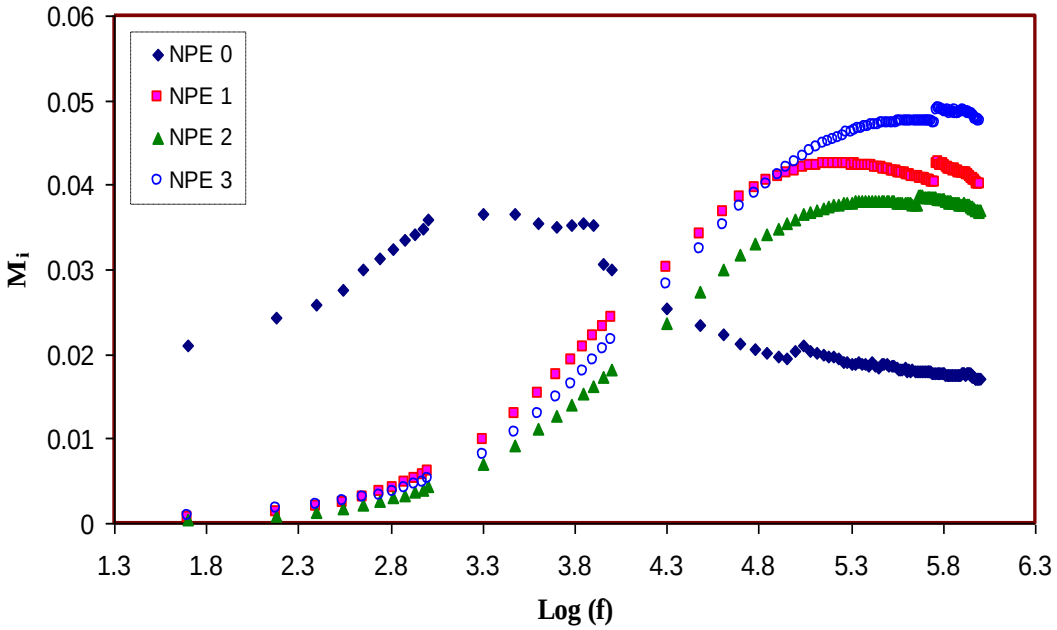

Figure 7. The imaginary part of electric modules (M_i) as a function of frequency, for all the fabricated samples.

From imaginary part of electric modulus spectra, conductivity relaxation peaks can be observed as exhibited in *Fig. 7*. It may be noticed that the relaxation peak shifts towards higher frequency side with increasing $BaTio_3$ content up to 3 wt. % and then shifts backwards when 5 wt. % of $BaTiO_3$ is introduced. As a result, the relaxation time $(\tau_o = 1/\omega_{max})$ decreases with an increase in $BaTiO_3$ concentration. This decrease of relaxation time can be ascribed to the increase of ionic mobility in amorphous phase of the electrolytes sample. These peaks are the transition regions from long range ionic mobility (translation) to short range mobility (dipolar), in other word, the carriers are confined to potential wells being mobile over short distance at higher frequencies [29, 35]. The low frequency side of the peaks is the region where ions have enough time to re-orient themselves with the alternating electric field and eventually diffuse. Consequently, double capacitance layer results between the electrode and electrolyte film. This produces a high dielectric constant and thus a very small M_i is observed. On contrary, the high frequency side of the peak is the region where ions can perform local (re-orientation) motion only and produce dispersion in AC conductivity [36]. The existence of peak in M_i spectrum (Fig. 7) and the absence in ε" spectrum (Fig. 3) may be considered as a strong evidence for the fact of ionic and polymer segmental motions are coupled [37].

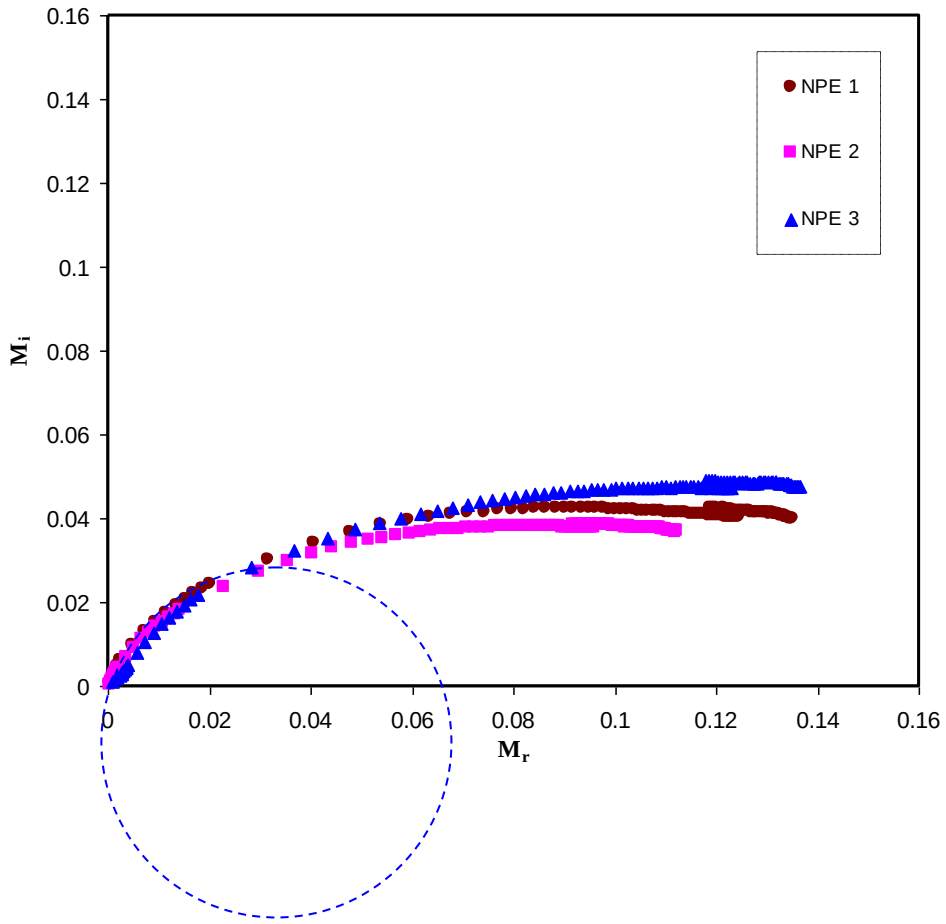

Figure 8. Argand plots for all the composite samples at ambient temperature.

Alternating current (ac) impedance spectroscopy has been commonly used to investigate the electrical properties of polymer ion conductors. The most common method employed in the study of

the ac response of a test system, i.e. an electrode-material arrangement. This can be carried out by the direct measurement of the impedance in the frequency domain. Various polarization and charge transfer processes which occur in a test system, over the measured frequency range can be studied [38]. *Fig. 8* shows the Argand plot (M_i versus M_r) for all the composite samples. It is obvious that Argand plots exhibits an incomplete half semicircle, revealing the non-Debye type relaxation process [19, 29]. At low frequency, the noticeable long tail is attributable to the large value of capacitance associated with electrode polarization [5]. From the studies of complex permittivity (see figures 2 and 3) the high value of dielectric parameters at low frequencies confirms aforementioned interpretation for the long tail of M_r and M_i at low frequency domain. From documented reports, it has been highlighted that as Argand plot shows semicircular behavior, the relaxation is either due to conductivity relaxation process or viscoelastic relaxation (or polymer molecular relaxation) [39, 40]. From the present work, as moreover, as the concentration of BaTiO3 increases, the Mi-Mr response departs from the absolute semicircular arc which ascribed to the increase in conductivity [4]. With an increase of BaTiO3 up to 3 wt.% the tail decreases while for 5 wt.% BaTiO3 the tail increases again. This shift of M_i-M_r curves towards the origin is caused by an increase of conductivity and a decrease of Zi and Zr ($M_i = \omega C_o Z_r$, $M_r = \omega C_o Z_i$).

3.4 DC Conductivity Study

From the Argand plots, one can see that the ion conductive mechanism includes segmental motion which is envisaged to be normal as reported for many polymer-based electrolytes. It is well reported that vehicle mechanism occurs in conventional liquid electrolyte systems [41, 42]. From this work, the conductivity of the samples (see Fig.9) are obviously close to each other, as a result, there is a small increment in conductivity for various amounts of BaTiO3 filler. The DC conductivity was calculated from the bulk resistances at various temperatures using the equation, $\sigma_{dc} = l/(R_b \times A)$, where l is the samples thickness, A is the electrode area and R_b is the bulk resistance obtained from impedance plots. This indicates that the interaction of the BT fillers with the polymer matrix is probably weak. It may act as a dissociation promoter in this polymer system; however, it might not change any intrinsic mechanism for the ionic conduction [43]. It can also be noticed from the plots that the temperature dependence of DC conductivity (σ_{dc}) shows nearly Arrhenius behavior at low temperatures (see region I) and a departure can be observed at high temperature region (see region II). The linear behaviors of DC conductivity may be related to the fact ionic transport occurred on the surface of the nano-particles or throughout a low-density polymer phase at the interfacial region, decoupling from the polymer relaxation mechanisms [44, 45].

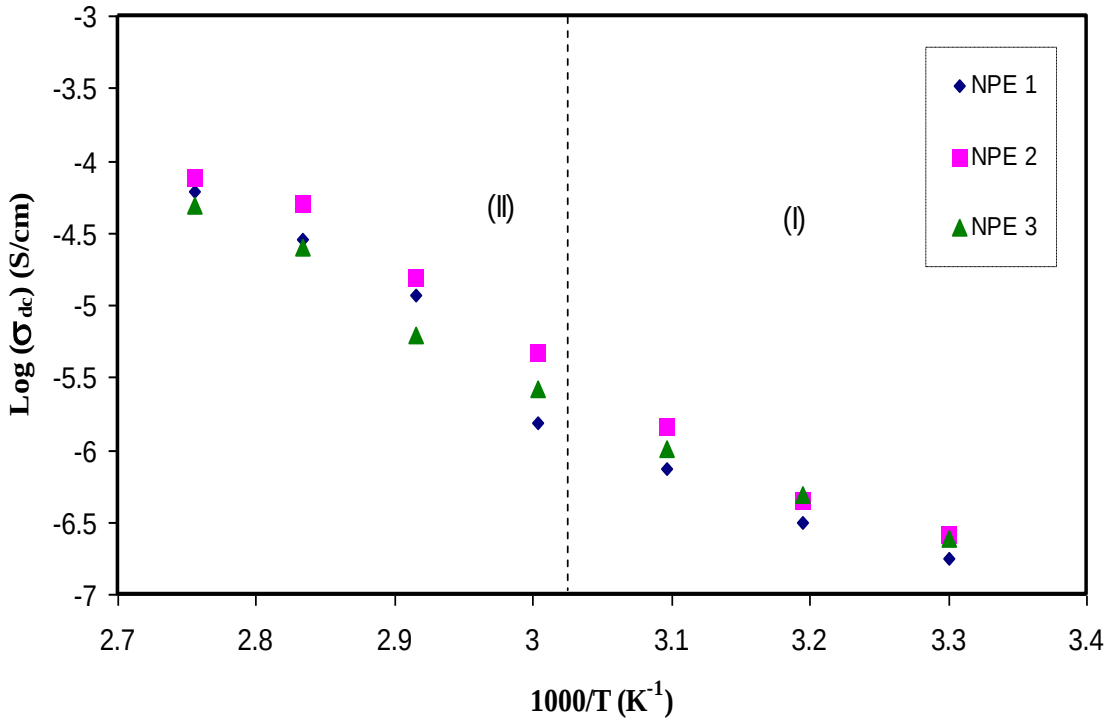

Figure 9. Temperature dependence of DC conductivity for composite samples

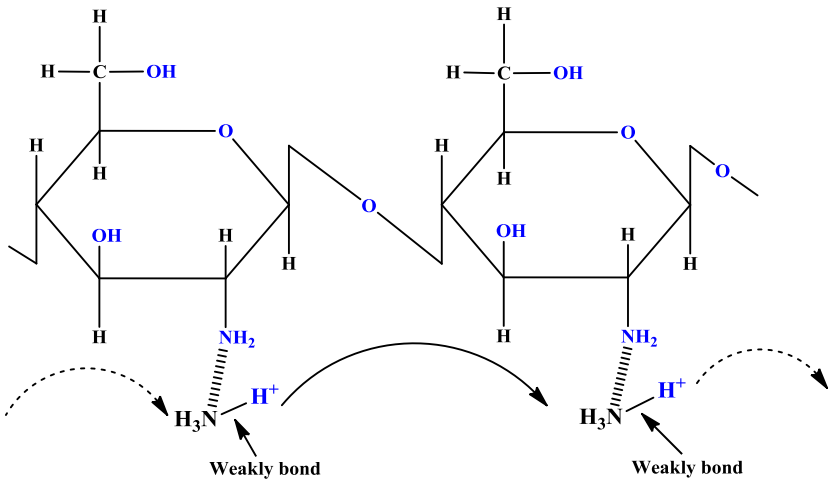

Scheme1. Mechanism of proton (H^+) ion conduction in chitosan based electrolyte

The observation of linear relationships between the σ_{dc} and 1000/T is an indicator for the fact that there is no phase transition in the polymer electrolyte at these temperature ranges and ion transport occurs through the hopping [46]. The expression hopping ascribed to the routine of rapid charge carrier displacement from one localized site to another nearby site [47]. Close coupling between the segmental motions of the chains and the ionic conductivity is responsible for the non-Arrhenius behavior of DC conductivity versus 1000/T at high temperature region [48, 49]. At high temperatures, the dielectric constant of the filler is not only increases, but also causes an increase of polymer segmental motion. Thus, the high dielectric constant of fillers may cause weakening the ionic bonding strength between the cation and anion of the salt, as a consequence, increase ion diffusivity in segment mobility due to

the suppression of polymer crystallization [41, 42]. It is clear that the room temperature conductivity of the samples is quite low. It is well reported that to reach high proton conductivity in polymer electrolytes, a high degree of hydration is necessary, as proton conductivity increases with elevating of both temperature and relative humidity (RH). In polymer electrolytes protons are transported via the Grotthuss mechanism. The movement of H^+ ion from one site to another; result in a vacancy that will be filled by another proton ion from a nearby neighboring site. This is the Grotthus mechanism where proton transport occurs through proton exchange between the polymer-salt complexed sites as depicted in scheme 1. The high mobility occurs at high RH and via the vehicle mechanism with lower mobility at low RH. In contrast, with increasing temperature, the vehicle mechanism progressively is dominating while as hydrogen bonds begin to elongate and break [10]. In this work, the value obtained for conductivity is comparable to that reported (7.8×10^{-7} S/cm) for chitosan incorporated with 30 wt. ammonium acetate (NH4CH3COO) [50].

4. CONCLUSIONS

In the present work, the effect of barium titanate (BaTiO3) nano filler on electrical and dielectric properties of proton conducting solid polymer electrolytes based on chitosan was discussed. The impedance plots shows that upto 3 wt.% BaTiO3 the conductivity can be increased. Similar trends of DC conductivity and dielectric constant versus BT concentration was explained. At low frequency high value for dielectric constant and dielectric loss was observed. Distinguishable peaks were observed in the imaginary part of electric modulus while no peaks observed in dielectric loss spectra. The relaxation processes was interpreted from the Argand plots. At low temperature the DC conductivity versus reciprocal of temperature follows the Arrhenius equation. The curvature of DC conductivity versus 1000/ T at high temperatures is an evidence for the fact that ion transport occurs with the help polymer segmental motion.

ACKNOWLEDGEMENT
The authors gratefully acknowledge the financial support for this study from Ministry of Higher Education and Scientific Research-Kurdistan Regional Government, Department of Physics, College of Science, University of Sulaimani, Sulaimani, and Komar Research Center (KRC), Komar University of Science and Technology, Sulaimani, 46001, Kurdistan Regional Government, Iraq.

References

1. M. Malathi, K. Tamilarasan, and V. Ganesan, *Polym. Compos.,* (2015) 42
2. J. Kumara, B. E. Henslee, and G. Subramanyam, *Solid State Batteries Abstract* MA2015-02 239 (2015)
3. W. Wang and P. Alexandridis, *Polymers,* 8 (2016) 387; doi:10.3390/polym8110387
4. S. B. Aziz and Z. H. Z. Abidin, *J. Appl. Polym. Sci.,* 132 (2015) 41774.
5. S. B. Aziz, *Adv. Mater. Sci. Eng.,* Volume 2016 (2016), Article ID 2527013, 11 pages, http://dx.doi.org/10.1155/2016/2527013

6. Z. Zhang, Q. Zhang, C. Ren, F. Luo, Q. Ma, Y.-S. Hu, Z. Zhou, H. Li, X. Huang, and L. Chen, *J. Mater. Chem. A,* 4 (2016) 15823
7. X.-L. Wang, A. Mei, M. Li, Y.-H. Lin, and C.-W. Nan, *J. Appl. Phys.*, 102 (2007) 054907
8. S. B. Aziz, Z. H. Z. Abidin, and M.F.Z. Kadir, *Phys. Scr.,* (2015) 035808
9. S. Y. Kim, S. Kim, and M. J. Park, *Nat. Commun.*, 1 (2010) 88
10. H. Gao and K. Lian, *RSC Adv.*, 4 (2014) 33091
11. M. Rikukawa and K. Sanui, *Prog. Polym. Sci.*, 25 (2000) 1463
12. R. Kumara, S. Sharma, D. Pathak, N. Dhimanb, and N. Arora, *Solid State Ionics* 305 (2017) 57
13. S. Navaratnam, K. Ramesh, and W. J. Basirun, *Mater. Res. Innovations,* 15 (2011) S184
14. X. Judez, H. Zhang, C. Li, Gebrekidan G. Eshetu, Y. Zhang, J.A. Gonzalez-Marcos, M. Armand, and L. M. Rodriguez-Martinez, *J. Phys. Chem. Lett.*, 8 (2017) 3473
15. M. M. Nasef, H. Saidi, and K.Z.M. Dahlan, *Nucl. Instrum. Methods Phys. Res., Sect. B,* 265 (2007) 168
16. Z. E. Biskeri, H. Rached, M. Bouchear, D. Rached, and M.S. Aida, *J. Electron. Mater.,* 45 (2016) 5082
17. S. B. Aziz, Z. H. Z. Abidin, and A. K. Arof, *Physica B* 405 (2010) 4429
18. S. B. Aziz, S. M. Mamand, S. R. Saed, R. M. Abdullah, and S. A. Hussein, *J. Nanomater.*, 2017 (2017), Article ID 8140693, 9 pages, https://doi.org/10.1155/2017/8140693
19. S. B. Aziz, O. Gh. Abdullah, and M. A. Rasheed, *J. Mater. Sci. Mater. Electron.*, 28 (2017) 2873
20. S. B. Aziz, M. A. Rasheed, and Z. H.Z. Abidin, J. Electron. Mater., 46 (2017) 6119
21. S. B. Aziz, Bull. Mater. Sci., 38 (2015) 1597
22. S. Das and A. Ghosh, *AIP Conference Proceedings* 1731 (2016) 110012
23. N. Kulshrestha, B. Chatterjee and P. N. Gupta, *High Perform. Polym.,* 26 (2014) 677
24. S. B. Aziz and Z. H. Z. Abidin, *Mater. Chem. Phys.*,144 (2014) 280
25. D. K. Pradhan, R. N. P. Choudhary, and B. K. Samantaray, *Mater. Chem. Phys.*, 115 (2009) 557
26. D. K. Pradhan, R. N. P. Choudhary, and B. K. Samantaray, *Int. J. Electrochem. Sci.,* 3 (2008) 597
27. S. B. Aziz, M.F.Z. Kadir, and Z.H.Z. Abidin, *Int. J. Electrochem. Sci.*,11 (2016) 9228
28. R. Kumar, A. Subramania, N.T. Kalyana Sundaram, G. Vijaya Kumar, and I. Baskaran, *J. Membr. Sci.,* 300 (2007) 104
29. S. B. Aziz, *Appl. Phys. A*, 122 (2016) 706
30. M. A. K. L. Dissanayake, P. A. R. D. Jayathilaka, R. S. P. Bokalawala, I. Albinsson, and B.-E. Mellander, *J. Power Sources,* 119–121 (2003) 409
31. H. Smaouia, L. E. L. Mirc, H. Guermazib, S. Agneld, and A. Toureille, *J. Alloys Compd.,* 477 (2009) 316
32. S. B Aziz, O. Gh. Abdullah, S. A. Hussein, and H. M. Ahmed, *Polymers* 9 (2017) 622
33. S. B. Aziz, Z. H. Z. Abidin, and A. K. Arof, *eXPRESS Polym. Lett.*, 4 (2010) 300
34. S. L. Agrawal, M. Singh, M. Tripathi, M. M. Dwiedi, and K. Pandey, *J. Mat. Sci.,* 44 (2009) 6060
35. J. Castillo, M. Chacon, R. Castillo, R. A. Vargas, P. R. Bueno, and J. A. Varela, *Ionics* 15 (2009) 537
36. M. M. Ahmad, *Nanoscale Res. Lett.*, 10 (2015) 58
37. A. S. Ayesh, *J. Thermoplast. Compos. Mater.*, 21 (2008) 309-322
38. D. C. Sinclair, *Bol. Soc, Esp. Cerám. Vidrio,* 34 (1995) 55
39. A. S. Ayesh, *Chinese J. Polym. Sci.*, 28 (2010) 537.
40. K. Mohomed, T.G. Gerasimov, F. Moussy, and J. P. Harmon, *Polymer* 46 (2005) 3847
41. D.-J. Youa, Z. Yina, Y.-k. Ahna, S. Choa, H. Kima, D. Shinb, J. Yooa, and Y. S. Kim, *J. Ind. Eng. Chem.*, 52 (2017) 1
42. W. Liu, S. W. Lee, D. Lin, F. Shi, S.Wang, A. D. Sendek, and Y. Cui, *Nat. Energy* 2 (2017) 17035
43. M. M. Varishetty, W. Qiu, Y. Gao, and W. Chen, *Polym. Eng. Sci.*, 50 (2010) 878
44. X. Hu, G. Hou, M. Zhang, R. Zhang, W. Ruan, and Y. Huang, *J. Solid State Electrochem.,* 20 (2016) 1845

45. S. B. Aziz, *Iran. Polym. J.*, 22 (2013) 877
46. S. B. Aziz, O. Gh. Abdullah, M. A. Rasheed, and H. M. Ahmed, *Polymers* 9 (2017) 187
47. S. B. Aziz, R. M. Abdullah, M. A. Rasheed, and H. M. Ahmed, *Polymers* 9 (2017) 338
48. M. Marzantowicz, J.R. Dygas, F. Krok, Z. Florjan´czyk, and E. Zygadło-Monikowska, *J. Non-Cryst. Solids*, 353 (2007) 4467
49. S. B Aziz, T. J. Woo, M. F. Z. Kadir, and H. M. Ahmed, *J. Sci.: Adv. Mater. Devices*, xxx (2018) 1, https://doi.org/10.1016/j.jsamd.2018.01.002
50. S. S. Alias, S. M. Chee, and A. A.Mohamad, *Arabian J. Chem.*, 10 (2017) S3687